

## Electrochemical Behavior of Self-Assembly Monodisperse Nanogels Based on Poly (vinyl alcohol) / Poly (acrylic acid) Semi- Interpenetrating Networks

Ayman M. Atta<sup>1,2,\*</sup>, Gamal A. El-Mahdy<sup>1,3</sup>, Hamad A. Al-Lohedan<sup>1</sup>, Ashraf M. El-saeed<sup>2</sup> and Ahmed M. Tawfeek<sup>4</sup>

<sup>1</sup> King Saud University, Surfactants research chair, Chemistry Department, College of Science, P.O.Box-2455, Riyadh-11451, Saudi Arabia.

<sup>2</sup> Petroleum Application Department, Egyptian Petroleum Research Institute, Cairo 11727, Egypt

<sup>3</sup> Chemistry Department, Helwan University, Helwan, Cairo 11795, Egypt.

<sup>4</sup> College of Science, King Saud University, Riyadh, Saudi Arabia

\*E-mail: [khaled\\_00atta@yahoo.com](mailto:khaled_00atta@yahoo.com)

*Received:* 31 October 2014 / *Accepted:* 19 December 2014 / *Published:* 24 February 2015

---

A new class of monodisperse water-soluble nanogels was prepared by a simple and green method. Semi-interpenetrating nanogels based on poly (vinyl alcohol), PVA, and poly(acrylic acid), PAA, nanoparticles. PAA was prepared by crosslinking of acrylic acid (AA) in the presence of hydroxypropylcellulose (HPC), N,N-methylenebisacrylamide (MBA) as a crosslinker and potassium peroxydisulfate (KPS) as redox initiator system. PVA nanoparticles were prepared by crosslinking in divinyl sulfone via changing the water and acetone compositions. PVA/PAA nanogel was prepared using epichlorohydrin as crosslinker. The structure and morphology of the nanogel was characterized by Fourier transform infrared spectroscopy (FTIR), transmission and scanning electron microscopy (TEM and SEM). The particle size of the prepared nanogel was determined by dynamic light scattering (DLS) measurements. The corrosion protection effect of PVA/PAA nanogel on the steel surface in 1M HCl solution was investigated using potentiodynamic polarization and electrochemical impedance spectroscopy (EIS). Polarization curves indicate that PVA/PAA nanogel is a mixed type inhibitor affecting both cathodic and anodic corrosion currents. The diameter of the capacitive loop increases substantially with increasing PVA/PAA nanogel concentration indicating that the corrosion resistance of steel has been enhanced significantly. The investigated inhibitor has shown good inhibition efficiency in 1 M HCl. The inhibition efficiency, calculated from impedance results showed the same trend as those obtained from potentiodynamic polarization measurements.

---

**Keywords:** Semi-interpenetrating nanogels; poly(acrylic acid); poly (vinyl alcohol); corrosion inhibition; monodisperse; potentiodynamic polarization.

## 1. INTRODUCTION

Iron and steel alloys are widely used in transportation and storage of petroleum crude oils because of their mechanical properties, excellent thermal and electrical conductivity, malleability, ductility, etc. However; they still tend to corrode in different media, especially in the presence of halide ions [1]. Now nanotechnology provides different chemical treatments used to provide additional long-term corrosion protection such as pretreatment of steel, coating, painting and using of corrosion inhibitors [2-5]. One of the most effective long term corrosion inhibitors is self-healing materials which can suppress corrosion initiated at the coating defects [6]. The nanoparticles can absorb the inhibitor during the preparation procedure and then slowly release them in contact with moisture. This way can provide a prolonged release of the inhibitors and also decrease the negative effect of the inhibitor ions on the hybrid film stability [7]. Nowadays, application of self-assembly nanoparticles as corrosion inhibitors attracts much attention due to their spontaneously chemical adsorption on metal surface which can prevent corrosive ions from transferring to the metal surface so that it can protect the metal from corrosion effectively [8-13]. Some researches concerning the protection of iron against corrosion by covering with ultrathin films [14, 15]. They prepared self-assembled monolayers on iron and investigated the protective ability of the monolayers. It has also been reported that using self-assembly technique can enhance the resistance against corrosion of iron [16].

The self-assembly nanogel materials have gained much attention due primarily to the novel properties depending on their sizes and aspect ratios [17]. In the past few years, there are different methods used for synthesizing self-assembly nanogels using emulsion polymerization technique besides the conventional physical and chemical methods [19-21]. Gels are usually formed by the free radical polymerization of monomers in the presence of a difunctional crosslinking agent and can be prepared either in bulk or in nano- or microparticles. In previous works [22-25], we succeeded to prepare self-assembled nanogels using free surfactants technique due to complexity of emulsion prepared nanogel methods. In this respect, the present work aims to prepare a new class of gels with two levels of structural, firstly preparing primary crosslinked polymer network chains as individual particle, while the secondary network is a system of crosslinked nanoparticles. It was expected that these gels will have new and unique properties including a high surface area and high affinity to form self-assembly layer at surface of different substrates. Moreover, it was expected that the using of self-assembled nanogel particles in the field of corrosion inhibition protection for steel can produce uniform thin film to cover all surface without any defects which provide advantages over normal organic inhibitors. The poly(vinyl alcohol), PVA, and poly(acrylic acid), (PAA), nanoparticles were prepared as individual particles followed by chemical crosslinking to prepare PVA-HPC nanogel. The corrosion

## 2. EXPERIMENTAL

### 2.1. Materials

Hydroxypropylcellulose (HPC) powder (average  $M_w = 1.0 \times 10^5$ ), acrylic acid monomers (AA, 99%), N,N'-methylenebisacrylamide (MBA, crosslinker), ammonium persulfate (APS, 99%, initiator),

N,N,N',N'-tetramethylethylenediamine (TEMED) divinylsulfone (DVS), and epichlorohydrine (EC) were all purchased from Sigma–Aldrich Chemical Co. and used as received. PVA (88 mol.-% hydrolyzed, MW ~ 25 000) was purchased from Polysciences, Inc. The working electrode was prepared from a steel rod with a chemical composition (in wt%) as follows: 0.14% C, 0.57% Mn, 0.21% P, 0.15% S, 0.37% Si, 0.06% V, 0.03% Ni, 0.03% Cr and the and Fe as balance. Before electrochemical measurements, the steel electrode was abraded with a series of emery papers of different grades (200, 400, 600, 800, 1000 and 1200, 2000) then washed in bi-distilled water degreased ultrasonically in ethanol, and finally dried at room temperature before being immersed in the test solutions. Hydrochloric acid was of analytical grade grade 37% HCl. All solutions were prepared with bi-distilled water

## 2.2. Preparation Methods:

### 2.2.1. Preparation of PVA nanoparticles:

The PVA nanoparticles were prepared using a surfactant-free method. PVA ( 2 g ) was dissolved in distilled water. Sodium hydroxide solution (5 M) was added to yield 2 wt.-% PVA solutions at pH 12. Acetone (30 mL) was added to 50 g PVA solution. The solution was stirred for 30 min followed by addition of 0.1 mL of DVS to the solution. The reaction was carried out for 4 h and the resulting nanoparticle dispersion was dialyzed five times and separated by ultracentrifuge at 15,000 rpm.

### 2.2.2. Preparation of PAA nanoparticles:

Poly (acrylic acid), PAA, nanogel was prepared by dissolving 1 wt% HPC in deionized water at room temperature under gentle stirring for 3–4 days. The AA( 1 g), MBA ( 0.3 g), APS (0.1 g) were added to HPC solution and stirred under nitrogen for 40 min at temperature of 30 °C. TEMED ( 0.1 g ) was added to initialize polymerization of PAA, which was then proceeded for 1 h. The unreacted AA, BIS, and TEMED were removed by dialyses to produce PAA nanogels for 7 days. The aqueous dispersion of the PAA nanogels was neutralized to pH = 7 by 5 M NaOH. PAA nanoparticle was separated from solution by freeze- drying.

### 2.2.3. Preparation of PVA/PAA nanogel

PVA (1 g), PAA ( 1 g) nanoparticles and EC ( 0.5 mL) were redispersed in 50 mL of aqueous NaOH solution (5 M) at pH 12. After incubation at 98 °C for 10 h, crosslinking among hydroxyl groups (PVA), epichlorohydrin and PAA (carboxyl groups) occurred and the nanogel formed a network. The PVA/PAA nanogel was separated by precipitation in acetone.

### 2.3. Characterization:

FTIR spectra were analyzed with a Nicolet FTIR spectrophotometer and all samples were ground and mixed with KBr and then pressed to form pellets.

High resolution transmission electron microscopy (HR-TEM) images for the prepared nanoparticles were recorded using (JEM-2100F, JEOL, Japan) at an acceleration voltage of 200 kV.

SEM images were taken with Gemini microscope DMS-982 (Zeiss, Germany). Samples were prepared from diluted dispersions of microgel in distilled water (100 $\mu$ g/ml) in aluminium foils to form a bigger droplet of aqueous dispersion and covered with a glass Petri-dish, dried at 37 °C over night. Small pieces of dried films were cut and placed on the SEM sample stage and coated with gold to increase the contrast and quality of the images.

Particle size measurements were performed using a dynamic light scattering (DLS) instrument a Nicomp<sup>TM</sup> model 380 particle sizing system with software version C-370 V-1.51a, and equipped with a fixed 90° external fiber angle and a 632.8 nm, 5 mW He-Ne laser.

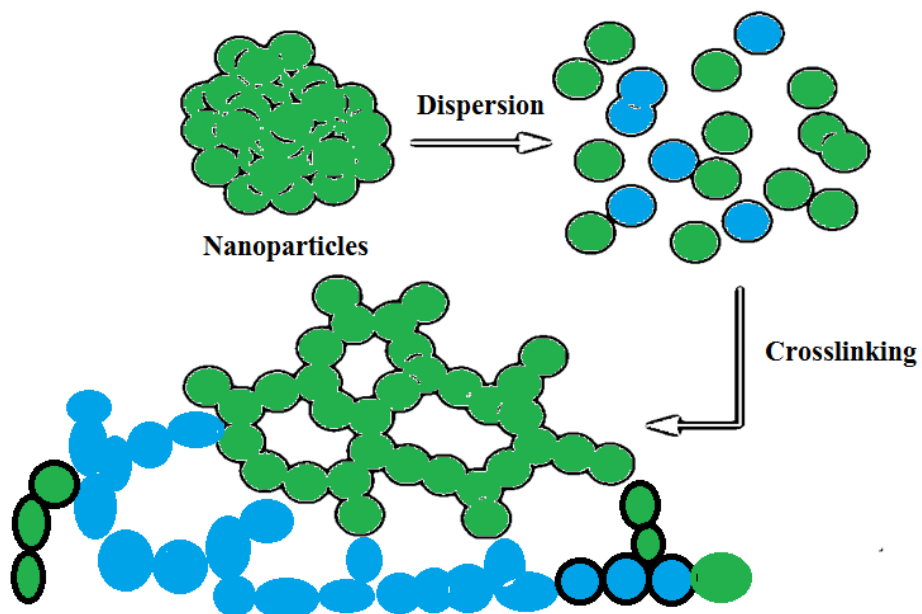
### 2.4. Electrochemical measurements

A platinum sheet was utilized as the counter electrode and saturated calomel electrode (SCE) as reference electrode. All electrochemical experiments were measured in a three-electrode cell. EIS was measured in the frequency range from 0.01 Hz to 10 kHz. The impedance data were analyzed using Zplot and ZView software. The impedance plots were fitted with a compatible equivalent circuit. The polarization curve was conducted with the scan rate set at 1 mV/ s. All electrochemical experiments were carried out with a SI 1287 Solartron (potentiostat/galvanostat) and Solartron 1260 as frequency response analyzer.

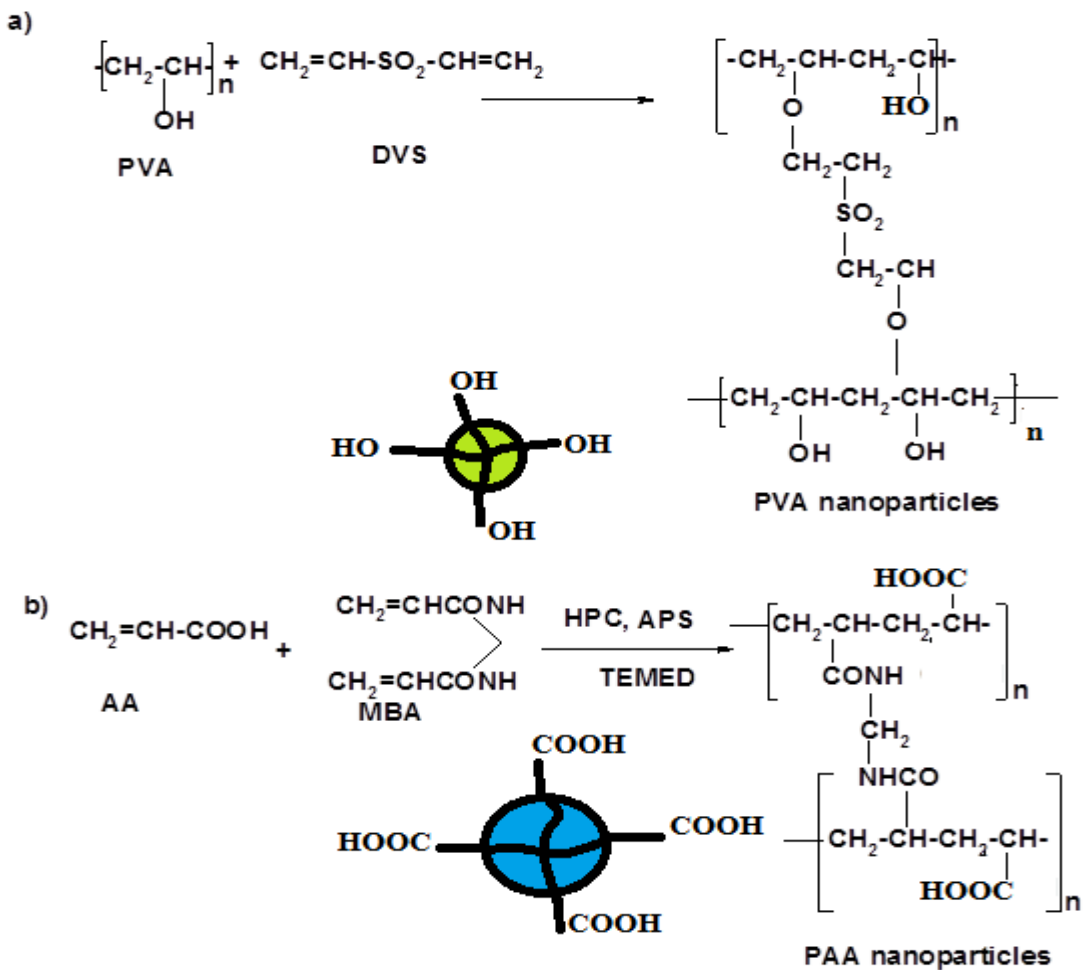
## 3. RESULTS AND DISCUSSION

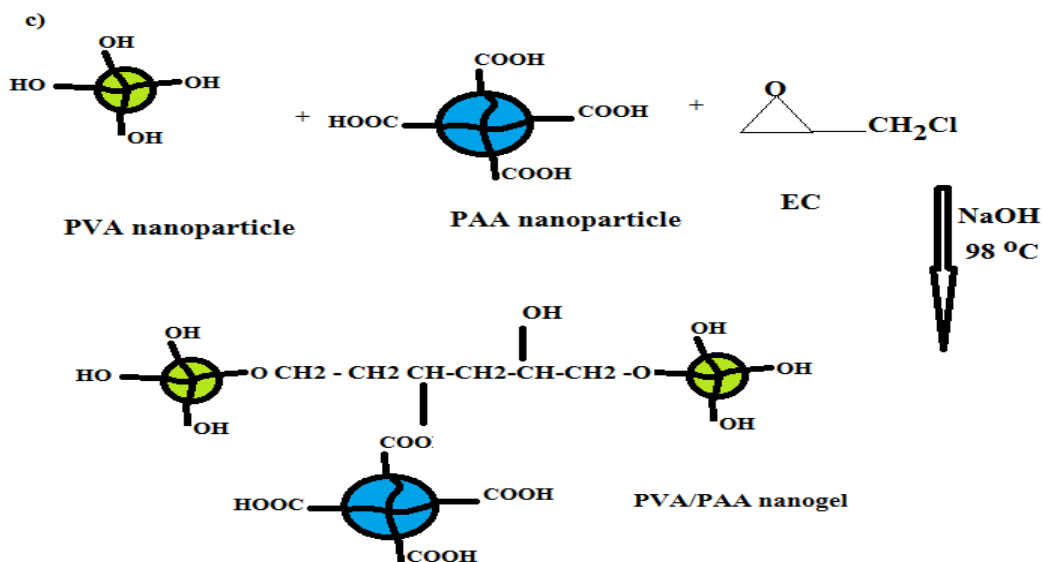
It is well known that there are a lot of limitations arise from preparing the nanogels by using of surfactants in the suspension and emulsion [26-27]. It is very difficult to completely remove organic solvent and surfactant from resulting nanogels. In this respect, the present work aims to prepare PVA and PAA nanogel using green method. The strategy of preparation can be illustrated in scheme 1.

It is based on preparing primary network by crosslinking two different types of nanoparticles individually. It is used as basic building blocks for synthesis of co-nanoparticle networks. The nanoparticles were dispersed and crosslinked and bonded with covalent bonds to form secondary network to produce monodisperse nanogels. This strategy was used to prepare monodisperse self-assembly PVA/PAA nanogel as represented in scheme 2.



Scheme 1. Schematic presentation of crosslinked nanogels.



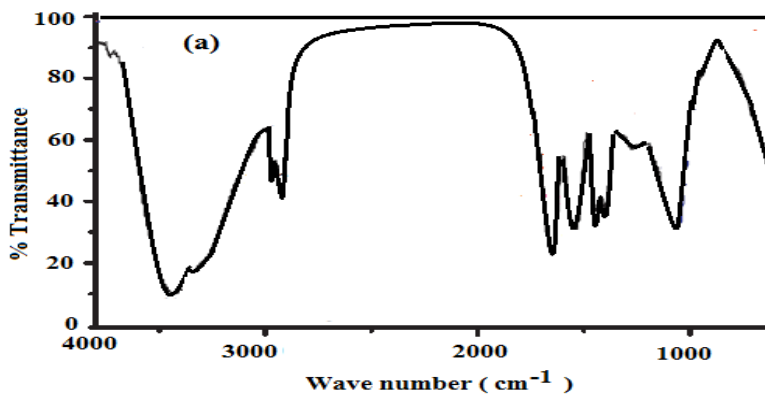


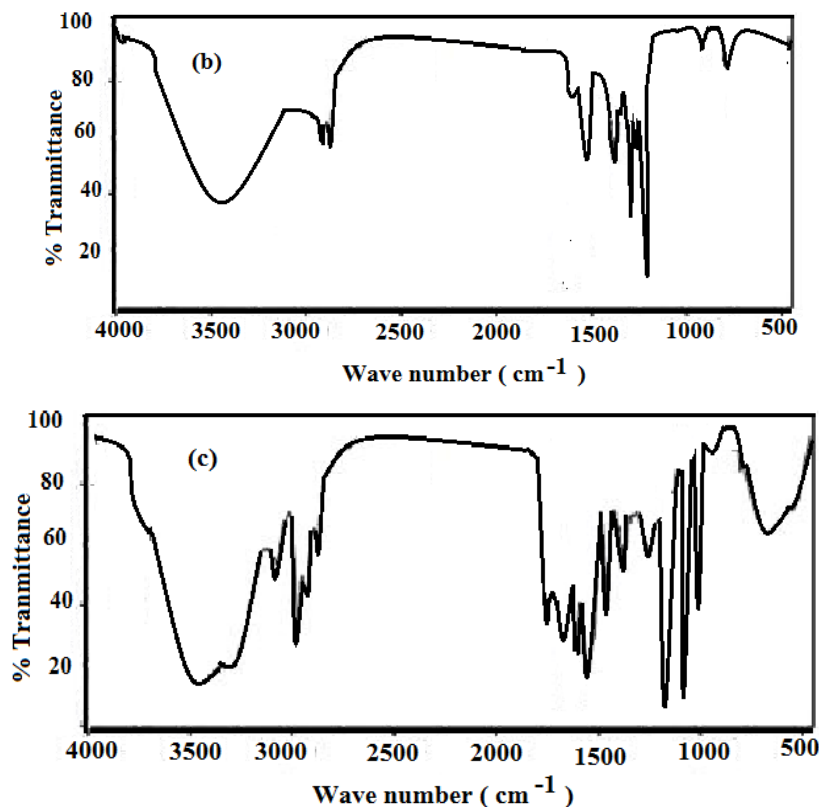
Scheme 2. Synthesis of PVA/PAA nanogel.

PVA was crosslinked using DVS and the nanoparticle was formed due to PVA collapse in the solvent water / acetone mixture [28, 29]. Moreover, it was expected that PAA hydrogel can be formed during preparation of PAA nanoparticles using radical polymerization as described in the experimental section [30]. It was previously reported that the HPC can form hydrogen bond with AA monomer at temperature below 41 °C and increased the hydrophobic interaction between HPC which produced nanogel without the formation of hydrogels [31]. The covalent crosslinking of PVA and PAA nanoparticles was carried out in the presence of EC and NaOH which produced covalent bonds between COOH groups of PAA and hydroxyl group of PVA nanoparticles to produce PVA/PAA nanogel (scheme 2 c).

### 3.1. Characterization of PVA/PAA nanogels

The chemical structure of PAA , PVA nanoparticles and PVA/PAA nanogels was determined from FTIR spectra represented in Figure 1.



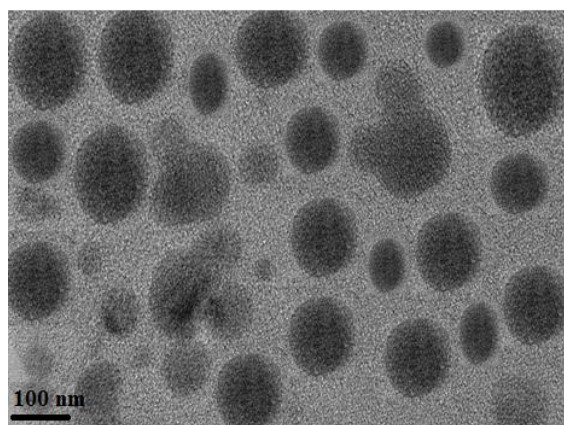
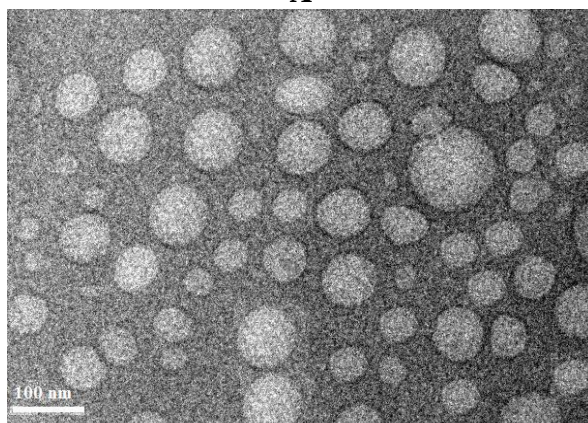
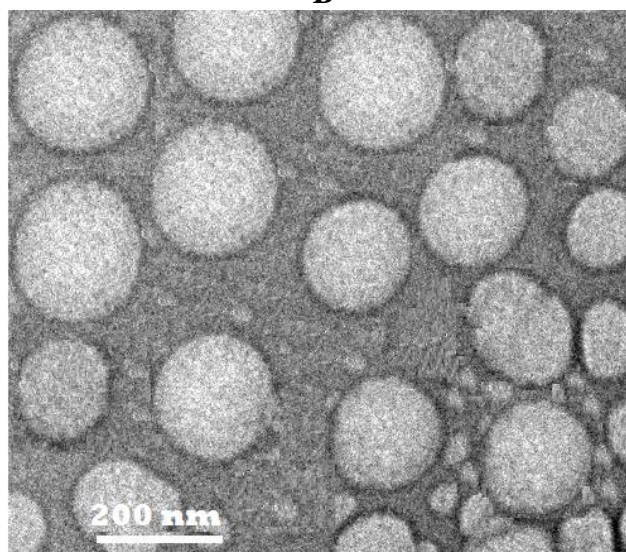


**Figure 1.** FTIR spectra of a) PAA, b) PVA and c) PVA/PAA nanogels.

The absorption band at  $3427\text{ cm}^{-1}$  showed that the hydroxyl group existed in the deprotonated PAA nanoparticles (figure 1a) at  $\text{pH} = 6.3$  which corresponds to the hydroxyl group of HPC embedded in the PAA nanoparticles. However, due to the ionization of the carboxyl group of PAA nanoparticle, the absorption bands at  $1651$  and  $1538\text{ cm}^{-1}$  are attributed to carbonyl groups and carboxylate ions, respectively [32]. These data indicated the formation of semi-interpenetrating structure of HPC with chemically crosslinked PAA nanogel networks. Figure 1 b and c indicated the appearance of new absorption band at  $1130\text{ cm}^{-1}$  which referred to  $-\text{SO}_2$  of DVS. Moreover the disappearance of absorption bands at  $3050\text{ cm}^{-1}$  indicated that the crosslinking polymerization of AA and MBA for PAA and PVA/PAA nanogel. It was also observed that new bands at  $1740\text{ cm}^{-1}$  appeared in spectrum of PVA/PAA nanogel (Figure 1 c) indicated the esterification of COOH group of PAA with EC.

The morphology of PAA, PVA nanoparticles and PVA/PAA nanogels can be illustrated from TEM and SEM micrographs. TEM is one of the most powerful analytical tools available which can give direct structural and size information of the nanoparticles. Figure 2 show the TEM picture of colloidal solutions of PAA, PVA nanoparticles and PVA/PAA nanogels which taken to determine the shape, size, and uniformity of the particles. TEM picture of the particles shows that these particles have distinct spherical structures, the spheres have different radius. TEM data indicated that the particle diameter changed from  $125\text{ nm}$ ,  $145\text{ nm}$  to  $200\text{ nm}$  for PAA, PVA and PVA/PAA, respectively. It is clear that the synthesized nanoparticles are uniform in size and non-aggregated. Figure 3 shows the SEM micrograph of PAA, PVA nanoparticles and PVA/PAA nanogels. The particles appeared as spheres join in filaments to form a continuous three-dimensional network. PVA

(Figure 3a) showed a broader particle size distribution more than PAA and PVA/PAA (Figure 3 b and c). Moreover, coagulation of nanogels is observed, which might be due to the surface tension effects caused by the drying process. The TEM and SEM studies demonstrate that the shape of the PVA/PAA nanogels can be completely controlled in order to obtain spherical nanoparticles with intermediate size.

**A****B****C**

**Figure 2.** TEM micrographs of a) PAA, b) PVA and c) PVA/PAA nanogels.

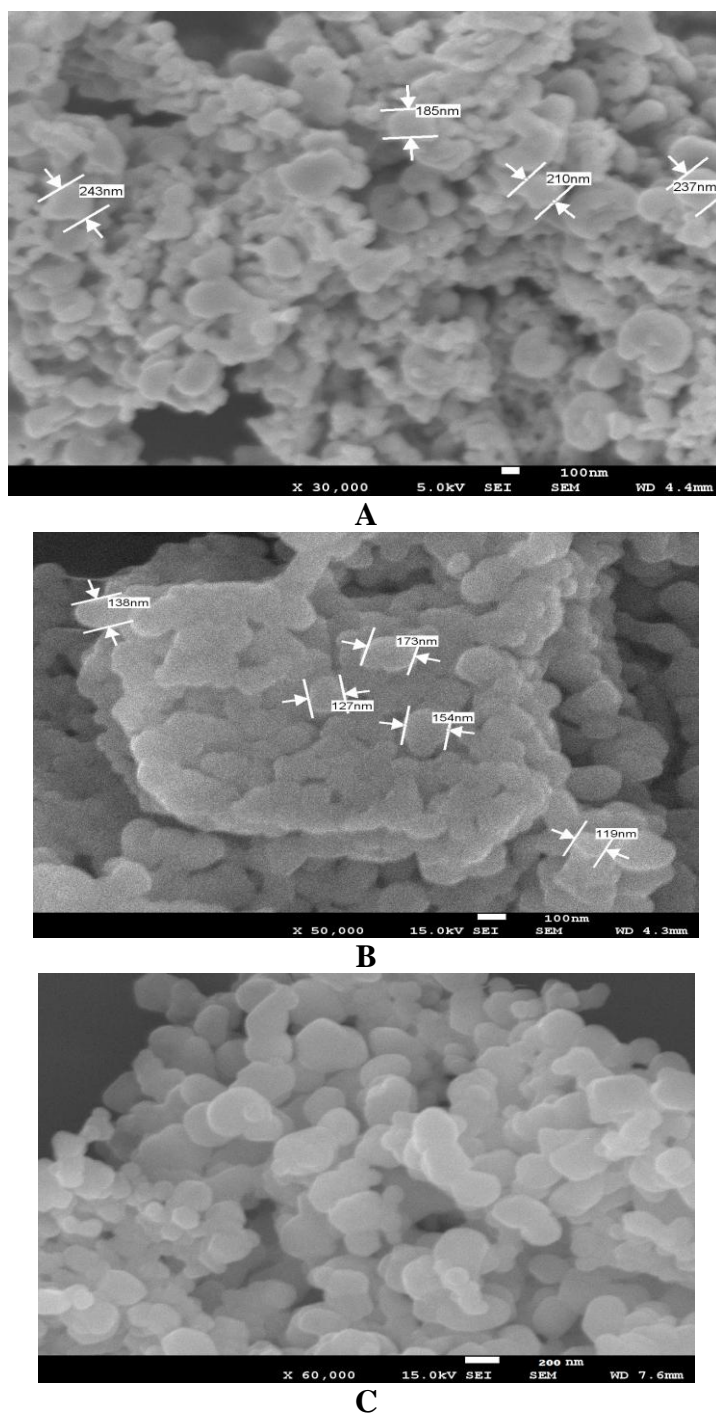


**Figure 3.** SEM micrographs of a) PAA, b) PVA and c) PVA/PAA nanogels

Image analysis on the TEM micrographs gives the ‘true radius’ of the particles (though determined on a statistically small sample), and Dynamic light scattering (DLS) provides the hydrodynamic radius on an ensemble average [33]. The technique of dynamic light scattering (DLS) has been widely employed for sizing nanoparticles in liquid phase. DLS has several advantages for sizing nanoparticles and has been widely used to determine the hydrodynamic size of various PVA, PAA and PVA/PAA as shown in Figure 4. This unique feature makes DLS one of the very powerful techniques in monitoring the colloidal stability of nanoparticle suspension. The obtained PVA, PAA

nanoparticles and PVA/PAA nanogel can easily be dispersed in aqueous media without aggregation. DLS measurements (figure 4) revealed that the nanoparticles are highly monodisperse in aqueous media. The size of PAA, PVA and PVA/PAA nanoparticles were 110, 85 and 210 nm, respectively. The polydispersity indexes (PDI) of PAA, PVA and PVA/PAA nanoparticles were 0.831, 0.341 and 0.038. These data indicated that the PVA and PVA/PAA formed monodisperse particles. Careful inspection of SEM, TEM data indicated that the size of particles are smaller than that obtained by DLS measurements although the DLS was carried out in water while SEM and TEM were obtained in dry state of nanoparticles. These were referred to fact that the particle larger than 100 nm, other factors such as electro viscous and surface roughness effects should be taken into consideration for the interpretation of DLS results [34].

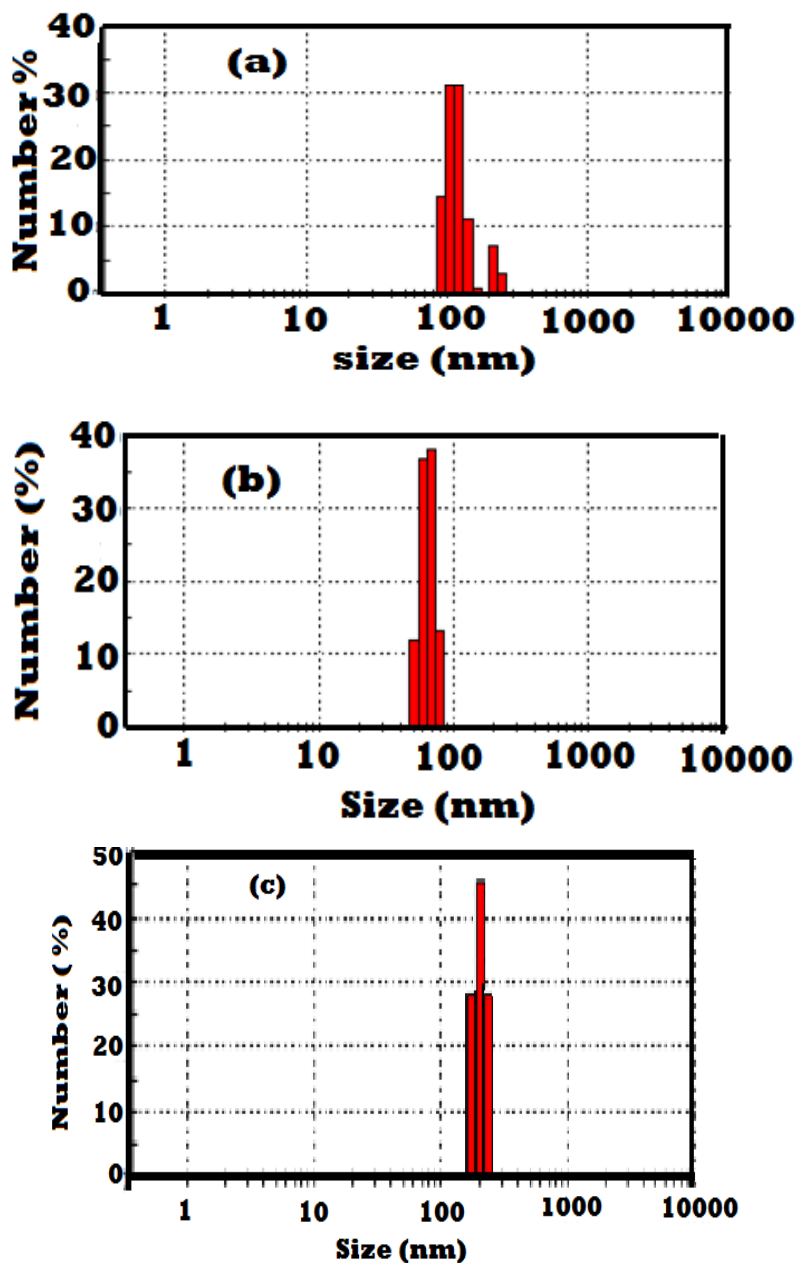


Figure 4. DLS measurements of PAA, PVA and PVA/PAA nanogels at 25 °C.

3.2. Electrochemical polarization studies

Figure 5 illustrates the potentiodynamic polarization curves of Steel in 1M HCl solution with different concentrations of PVA/PAA nanogel. The presence of PVA/PAA nanogel causes a prominent decrease in the corrosion rate i.e. shifts both anodic and cathodic curves to lower values of current densities at the same potential compared with those of the blank solution. The addition of PVA/PAA nanogel can effectively suppress anodic and cathodic reaction processes simultaneously. Hence, PVA/PAA nanogel acts as mixed-type corrosion inhibitor. It suppresses both anodic and cathodic reaction by adsorbing on the steel surface. This effect is attributed to the inhibitor adsorption on the active sites of the steel surface [35-40]. This suppression of the corrosion process may be the results of adsorbed PVA/PAA nanogel covering on the steel surface and decreasing reactive sites of steel surface area. Thus, the adsorbed PVA/PAA nanogel on steel surface acted as an effective barrier to the anodic dissolution and cathodic reduction reaction on steel surface, thereby protecting the steel surface from corrosion. The formation of, compact and protective layer on steel surface inhibits both the anodic dissolution and cathodic reduction of hydrogen. The decrease in the cathodic current densities may be attributed to the cathodic sites blockage by the inhibitors. Moreover, the PVA/PAA nanogel -changes the shape and slope of anodic branches noticeably. This finding clearly shows that the inhibitors reduced anodic dissolution rate of steel by forming protective films on the anodic sites. Table 1 lists the electrochemical parameters, including corrosion potential ( $E_{corr}$ ) corrosion current density  $i_{corr}$ , cathodic ( $b_a$ ) and anodic Tafel slopes ( $b_a$ ). The inhibition efficiency was calculated using the following equation[41-42]:

$$IE\% = 1 - i_{corr (inh)} / i_{corr}^o \times 100 \tag{1}$$

where  $i_{corr (inh)}$  and  $i_{corr}^o$  are corrosion current densities in the presence and absence of inhibitor, respectively. The values of IE% with different inhibitor concentrations are listed in Table 1. The value of IE% regularly increase with the increasing inhibitor concentration (Table 1). As the inhibitor concentration increases, the barrier property of protective layer becomes more efficient.

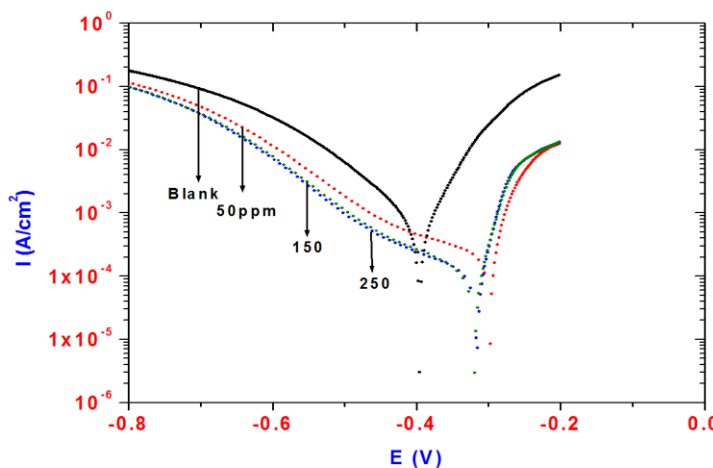


**Figure 5.** Polarization curves of steel in 1M HCl solution containing different concentrations of PVA/PAA nanogel.

**Table 1.** Inhibition efficiency values for steel in 1M HCl with different concentrations of PVA/PAA nanogel calculated by Polarization and EIS methods.

|         | Polarization Method |         |                       |   |       | EIS Method            |                           |       |
|---------|---------------------|---------|-----------------------|---|-------|-----------------------|---------------------------|-------|
|         | Ba (mV)             | Bc (mV) | E <sub>corr</sub> (V) | i <sub>corr</sub> (μA/cm <sup>2</sup> ) | IE%   | R <sub>Ct</sub> (Ohm) | Cdl (μF/cm <sup>2</sup> ) | IE%   |
| Blank   | 69                  | 120     | -0.3955               | 839                                     | _____ | 1.80                  | 334                       | _____ |
| 50 ppm  | 51                  | 359     | -0.2993               | 254                                     | 69.7  | 6                     | 181                       | 70.0  |
| 150 ppm | 54                  | 277     | -0.3198               | 148                                     | 82.3  | 10.9                  | 137                       | 83.4  |
| 250 ppm | 51                  | 281     | -0.3165               | 137                                     | 83.6  | 11.5                  | 130                       | 84.3  |

Summarizing the results of polarization curves and electrochemical parameters listed in Table 1, it can be seen that the values of I<sub>corr</sub> and %IE are greatly decreased with increasing PVA/PAA nanogel concentration, and the cathodic tafel slope is shifted to a great extent in presence of the PVA/PAA nanogel on the steel surface. From Table 1 we find that the inhibition efficiency (IE%) of the PVA/PAA nanogel steel electrode reach 83.4% as its concentration of solution at 250ppm and It is inferred that the formation of inhibitive film on Steel surface mainly controls the the corrosion process of steel in acidic solution. These results are indicative of the adsorption of inhibitor on the surface of steel with a formation of protective layer.

3.3. Electrochemical impedance spectroscopy measurements

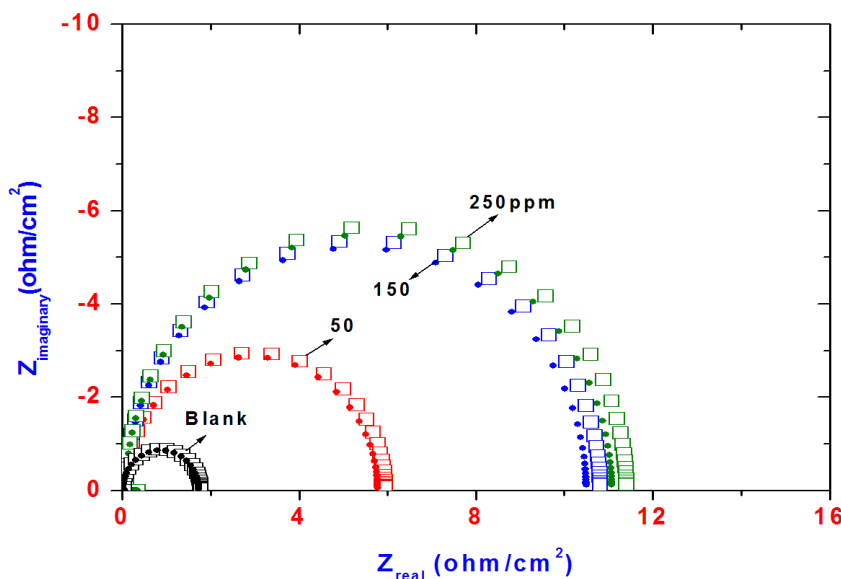


**Figure 6.** Nyquist diagram for steel in 1 M HCl solution containing PVA/PAA nanogel

The influence of PVA/PAA nanogel concentration on the Nyquist plots of steel electrode in aerated 1 M HCl solution is depicted in Fig.6. In all cases, the Nyquist plots are not perfect semicircles. This phenomenon is related to the roughness and inhomogeneity of the electrode surface [43]. The semicircle in all cases corresponds to a capacitive loop.

The semicircle radii depend on the concentration of the PVA/PAA nanogel. The diameter of capacitive loop enlarges gradually with increasing the concentrations of the PVA/PAA nanogel, indicating the formation of protective film, which would be sufficiently densely packed to inhibit the corrosion of steel in acidic solution. It suggests that the addition of PVA/PAA nanogel in 1M HCl solution has significantly improved the corrosion resistance behavior of steel in 1M HCl solution. All the Nyquist plots are analyzed in terms of the equivalent circuits shown in Fig.7 and the fit parameters are listed in Table 1. The circuit consists of  $R_s$ , which represents the resistance of the solution between the working and the reference electrodes, CPE is Constant Phase Element and  $R_{ct}$  is the charge transfer resistance corresponding to the corrosion reaction at the steel/solution interface [44-45]. CPE is often used to fit the impedance behavior of the electric double layer instead of the pure capacitor. It is noticeable that  $C_{dl}$  decrease, while  $R_{ct}$  increase as the concentration of PVA/PAA nanogel increases. Charge transfer resistance is correlated to the corrosion current density for corrosion systems characterized by a charge transfer controlled process [46]. As seen from Table 1, the presence of PVA/PAA nanogel leads to the decrease in  $C_{dl}$  values. The decrease in  $C_{dl}$  values was caused by adsorption of PVA/PAA nanogel [47]. The data clearly showed also that when the PVA/PAA nanogel concentration increased,  $C_{dl}$  decreased. This behavior may be result from a decrease in local dielectric constant and/or an increase in the thickness of the electrical double layer, suggests that the licorice extracts function by adsorption at the metal-solution interface [48]. The impedance of a CPE is expressed as follows [49]:

$$Z_{CPE} = Q^{-1} (j\omega)^{-n}$$

where subscript  $Q$  is a CPE,  $j^2 = -1$  is an imaginary number, and  $\omega$  is the angular frequency ( $\omega = 2\pi f$ ). and  $n$  is the CPE exponent, which gives detail about the degree of surface inhomogeneity resulting from surface roughness, inhibitor adsorption, porous layer formation, etc. [50]. The value range of a real electrode of  $n$  is often between 0 and 1. On the basis of the value of the exponent  $n$ , CPE can represent resistance ( $n = 0$ ,  $Q = R$ ), capacitance ( $n = 1$ ,  $Q = C$ ), inductance ( $n = -1$ ,  $Q = L$ ) or Warburg impedance ( $n = 0.5$ ,  $Q = W$ ) The IE% was calculated using the following equation:

$$IE\% = 1 - R_{ct(1)} / R_{ct(2)} \times 100 \quad (2)$$

where  $R_{ct(1)}$  and  $R_{ct(2)}$  are the charge transfer resistances in the HCl solution in the absence and in the presence of the inhibitors, respectively. IE (%) values increased with increasing inhibitor concentration, which can be attributed to increasing inhibitor adsorption which decreases the exposed electrode surface area.

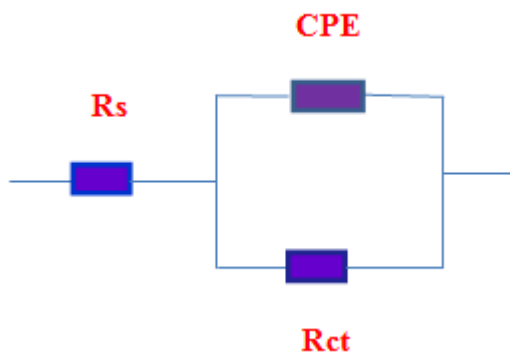


**Figure 7.** Equivalent circuit employed for fitting experimental data.

The significant increase in  $R_{ct}$  could be attributed to the decrease of active sites available for the steel dissolution reaction with increasing adsorption of PVA/PAA nanogel inhibitor on the steel surface. In addition, the water molecules at the steel/solution interface are replaced by the adsorbed PVA/PAA nanogel gradually, leading to a decrease in the local dielectric constant and thicker electric double layer, both of which cause decrease of  $C_{dl}$ . The inhibition efficiency, calculated from impedance results, showed the same trend as those obtained from potentiodynamic polarization measurements.

#### 4. CONCLUSIONS

1. New monodisperse semi- interpenetrating nanogel based on PVA/PAA was prepared .
2. Electrochemical results demonstrated that PVA/PAA nanogel effectively inhibited steel corrosion in 1M HCl solution.
3. Potentiodynamic polarization studies showed that PVA/PAA nanogel acted as a mixed-type inhibitor.
4. The inhibition efficiency increased with increasing the concentration of PVA/PAA nanogel and reached its maximal value at 250ppm concentration.
5. EIS measurement results indicate that the charge transfer resistance of the steel electrode increases greatly and its double capacitance decreases with increasing PVA/PAA nanogel concentration.
65. Data obtained from EIS measurements are in good agreement with those obtained from the potentiodynamic polarization study.

#### ACKNOWLEDGEMENT

The project was supported by King Saud University, Deanship of Scientific Research, Research Chair.

## References

1. D. Wang, G.P. Bierwagen, *Prog. Org. Coat.* 64 (2009) 327.
2. K.A. Yasakau, M.L. Zheludkevich, O.V. Karavai, M.G.S. Ferreira, *Prog. Org. Coat.* 63 (2008) 352.
3. S. M.Madani, M.Ehteshamzadeh, H. H. Rafsanjani, *Thin Solid Films* 519 (2010) 145–150
4. R. Joseph Rathish, R. Dorothy, R. M. Joany, M. Pandiarajan and Susai Rajendran, *Eur. Chem. Bull.*, 2 (2013), 965.
5. A.Mathiazhagan and R. Joseph, *Inter. J. Chem. Eng. Appl.*, 2 (2001) 225.
6. L.S. Kasten, J.T. Grant, N. Grebasch, N. Voevodin, F.E. Arnold, M.S. Donley, *Surf. Coat. Technol.* 140 (2001) 11.
7. M.L. Zheludkevich, R.Serra, M. F.Montemor, M.G.S. Ferreira *Electrochem. Comm.* 7 (2005) 836.
8. Z. Zhang a, S. Chen , H. Ren a, J. Zhou, *Appl. Surf. Sci.* 255 (2009) 4950.
9. G.K. Jannings, T.H. Yong, J.C. Munro, P.E. Laibinis, *J. Am. Chem. Soc.* 125 (2003) 2950.
10. A. Ulman, *Chem. Rev.* 96 (1996) 1533.
11. Y.H. Lai, C.T. Yeh, S.H. Cheng, P. Liao, W.H. Hung, *J. Phys. Chem. B* 106 (2002) 5438.
12. A. M. Atta, M. Hegazy, O. E. El-Azabawy, H.S. Ismail, *Corros. Sci.*, 53, 1680–1689 (2011).
13. G. A. El Mahdy, A.M. Atta, A. K. F. Dyab, H. A. Al-Lohedan, *Journal of Chemistry*, 2013 (2013), Article ID 125731, 9 pages.
14. T. Shimura, K. Aramaki, *Corros. Sci* 50 (2008) 1397.
15. Y.Y. Feng, S.H. Chen, W.J. Guo, Y.X. Zhang, G.Z. Liu, *J. Electroanal. Chem.* 602 (2007)115.
16. W.J. Guo, S.H. Chen, Y.Y. Feng, C.J. Yang, *J. Phys. Chem. C* 111 (2007) 3109.
17. M. Motornov, Y. Roiter, I. Tokarev, S. Minko, *Prog. Poly. Sci.* 35 (2010) 174.
18. D. Suzuki, S. Tsuji, H. J. Kawaguchi, *J Am Chem Soc* 129 (2007) 8088.
19. S.Y. Zhao, S.H. Chen, S.Y. Wang, D.G. Li, H.Y. Ma, *Langmuir* 18 (2002) 3315.
20. W.L. Cheng, S.J. Dong, E.K. Wang, *Electrochem. Comm.* 4 (2002) 412–416.
21. Z. Zhang, R.C. Petel, R. Kothari, C.P. Johnson, S.E. Friberg, P.A. Aikens, *J. Phys. Chem. B* 104 (2000) 1176.
22. A. M. Atta, R. A. M. El-Ghazawy, R. K. Farag, S. M. Elsaheed, *Poly. Adv. Technol.* . 22. (2011) 732.
23. A. M Atta, G. A. El-Mahdy, H. A. Al-Lohedan, A. O. Ezzat, *Molecules* 07/2014; 19:10410-10426
24. G. A. El-Mahdy, A. M. Attaa, H. A. Al-Lohedana, *J. Tai. Inst. Chem. Eng.*, 45 (2014) 1947.
25. A. M. Atta, A.K. F. Dyaba, and H. A. Allohedan, *Poly.Adv. Technol.*, 24, (2013) 986.
26. R.Pelton, *Adv. Collo. Interf. Sci* 85 (2000) 1.
27. K. Landfester, M. Willert, M. Antonietti, *Macromolecules* 33 (2000) 2370.
28. Z. Hu, X. Lu, J. Gao, C. Wang, *Adv. Mater.* 12 (2000) 1173.
29. R-S. Yao, Q-D. You, P-J. Liu, Y-F. Xu, *J. Appl. Poly. Sci.*, 111(2009) 358.
30. Q. Liao, Q. Shao, H. Wang, G.Qiu, X. Lu *Car. Poly.* 87 (2012) 2648.
31. M.A. Akl, A.A. Sarhan, K. R. Shoueir, A.M. Atta, *J. Disp. Sci. Technologies* 34 (2013) 1399.
32. Y. Hu, X. Jiang, Y. Ding, H. Ge, Y. Yuan, C. Yang, *Biomaterials* 23 (2002) 3193.
33. B.J. Berne, R. Pecora, *Dynamic Light Scattering: With Applications to Chemistry Biology and Physics*. New York: Dover Publications; 2000.
34. Gittings MR, Saville DA, *Colloid Surface A: Physiochem Eng Aspects* 141 (1998)111.
35. X. Li, S. Deng, H. Fu, G. Mu, *Corros. Sci.* 51 (2009) 620.
36. J. Aljourani, K. Raeissi, M.A. Golozar, *Corros. Sci.* 51 (2009) 1836.
37. I. Ahamad, R. Prasad, M.A. Quraishi, *Corros. Sci.* 52 (2010) 3033.
38. G.E. Badr, *Corros. Sci.* 51 (2009) 2529.
39. M. El Azhar, B. Memari, M. Traisnel, F. Bentiss, M. Lagrenee, *Corros. Sci.* 43 (2001) 2229.
40. R. Solmaz, *Corros. Sci.* 52 (2010) 3321–3330.
41. E. McCafferty, *Corros. Sci.* 47 (2005) 3202.

42. Q. Qu, L. Li, W. Bai, S. Jiang, Z. Ding, *Corros. Sci.* 51 (2009) 2423.
43. M.A. Deyab, S.T. Keera, *Mater. Chem. Phys.* 146 (2014) 406.
44. V.S. Reznik, V.D. Akamsin, Y.P. Khodyrev, R.M. Galiakberov, Y.Y. Efremov, L. Tiwari, *Corros. Sci.* 50 (2008) 392.
45. R.A. Prabhu, T.V. Venkatesha, A.V. Shanbhag, G.M. Kulkarni, R.G. Kalkhambkar, *Corros. Sci.* 50 (2008) 3356.
46. M.A. Deyab, S.S. Abd El-Rehim, *Corros. Sci.* 65 (2012) 309.
47. K. Aramaki, M. Hagiwara, H. Nishihara, *Corros. Sci.* 5 (1987) 487.
48. M.A. Deyab, *Corros. Sci.* 80 (2014) 359.
49. D.D. Macdonald, *Electrochim. Acta* 35 (1990) 1509.
50. L.J. Li, X.P. Zhang, J.L. Lei, J.X. He, S.T. Zhang, F.S. Pan, *Corros. Sci.* 63 (2012) 82.

© 2015 The Authors. Published by ESG ([www.electrochemsci.org](http://www.electrochemsci.org)). This article is an open access article distributed under the terms and conditions of the Creative Commons Attribution license (<http://creativecommons.org/licenses/by/4.0/>).